

# Screening of the Photon Field in Surface Photoemission from Simple Metals

S. Natschläger<sup>1</sup>, J. Alberich<sup>2</sup>, N. Barberán<sup>2</sup>, J. Bausells<sup>3</sup>, R. Ruppin<sup>4</sup> and C. Simó<sup>5</sup>

<sup>1</sup>*Institut für Theoretische Physik, Johannes Kepler Universität, A-4040 Linz, Austria*

<sup>2</sup>*Departament d'Estructura i Constituents de la Matèria, Facultat de Física, Universitat de Barcelona, E-08028 Barcelona*

<sup>3</sup>*Centro Nacional de Microelectrónica-CSIC, E-08193 Bellaterra (Barcelona), Spain*

<sup>4</sup>*SOREQ NRC, Yavne 81800, Israel*

<sup>5</sup>*Departament de Matemàtica Aplicada i Anàlisi, Universitat de Barcelona, E-08007 Barcelona, Spain*

## Abstract

A previous two-step hydrodynamic model calculation of angle-resolved photoemission has been improved by modeling the surface with a soft analytic function. The same ground-state potential is used to screen the photon field and to calculate the electronic wave functions. The implemented code can be used for arbitrary ground state densities along the perpendicular direction. Mathematical and physical aspects of the model are discussed extensively. The behavior of the main peak of the spectrum in response to the variation of some parameters leads us to the conclusion that the peak cannot be interpreted as the direct excitation of multipole modes. This conclusion was suggested in the previous two-step model calculation.

KEYWORDS: Surface waves; multipole surface plasmons; photoelectron emission.

PACS: 73.20.Mf, 73.50.Pz

## 1. Introduction

The subject of the interaction of external probes with metal surfaces, and the possibility of excitation of multipole modes, have attracted much attention. The multipole modes, which were first predicted theoretically by Bennett<sup>1</sup> in 1970, from the hydrodynamic model, have only recently been detected experimentally by inelastic electron scattering on Na, K, Cs and Ag surfaces.<sup>2-4</sup> Theoretical quantum-mechanical interpretations of these experiments, based on the random phase approximation and on the local density approximation, have been presented.<sup>2,3,5</sup> Although no multipole modes could be observed in electron scattering from Al surfaces, it was debated whether a peak which appears in the photoemission spectrum of Al<sup>6,7</sup> could be attributed to multipole modes.<sup>3,8,9</sup> To provide more insight into this question, theoretical calculations of the angle dependence of the photoemission spectrum are required. Here we present such a calculation, using a refined hydrodynamic model, into which a realistic surface density profile is incorporated.

Photoemission within a solid needs some linear momentum supplier besides the two components: the incoming photon and the emitted electron. An isolated electron cannot absorb a photon in a process that preserves total energy and momentum. Due to the fact that the electrons have a finite mean free path, the photon is absorbed near the surface. Within this region, the most important momentum suppliers in a simple metal are the step potential and the screened photon field.

These two contributions can be determined explicitly in a Hamiltonian formulation. The perturbation produced by the incident photon is given by

$$H_1 = -\frac{e}{2mc} (\mathbf{p} \cdot \mathbf{A} + \mathbf{A} \cdot \mathbf{p}), \quad (1)$$

where only terms up to first order in the vector potential  $\mathbf{A}$  are considered and where the gauge  $\Phi = 0$  ( $\Phi$  is the scalar potential) has been used.  $\mathbf{p}$  is the linear momentum operator and  $c$ ,  $e$ , and  $m$  are the velocity of light in vacuum and the electron charge and the mass, respectively. We will employ atomic units throughout the paper.

If  $|i\rangle$  and  $|f\rangle$  are two eigenstates of the unperturbed Hamiltonian  $H_0$  and  $\mathbf{A}$  is the external plus the induced field, the amplitude of the excitation probability is given (apart from constant factors) by:

$$\langle f | \mathbf{p} \cdot \mathbf{A} + \mathbf{A} \cdot \mathbf{p} | i \rangle = -i \langle \mathbf{f} | (\nabla \cdot \mathbf{A}) + 2\mathbf{A} \cdot \nabla | i \rangle. \quad (2)$$

While the first term on the right hand side is directly related to the spatial variation of the vector potential due to screening effects within the electron gas, the second term is related to the step potential at the vacuum-solid interface. This follows from the fact that for the unperturbed Hamiltonian  $H_0 = p^2/2m + V$  we have

$$\langle f | \nabla | i \rangle = \frac{1}{\mathbf{E}_i - \mathbf{E}_f} \langle \mathbf{f} | \nabla V | i \rangle. \quad (3)$$

Therefore, if  $\mathbf{A}$  is taken out before the integral in the second term of the right hand side of Eq. (2) (as in some approximations with optical photons), then the entire contribution to the momentum would come from the variation of the ground state potential at the surface. However, in a full calculation, as  $\mathbf{A}$  must be placed inside the bracket, the two effects (screening and inhomogeneities of  $V$ ) are mixed.

These two contributions to the excitation probability are connected with different kinds of processes during the electron emission: collective and single-particle excitations respectively.

The contributions connected with the potential gradient term,  $\nabla V$ , consist of individual electron-hole pairs created at the surface and of the subsequent emission of the electron. On the other hand, in the processes connected with the divergence of the vector potential the electron gas screens the incoming photon, producing surface collective excitations that supply the extra momentum.

Moreover, different types of collective excitations play different roles in photoemission. When the photon frequency is equal to  $\omega_p$ , the bulk plasma frequency, the amplitude of the vector potential is drastically reduced inside the metal and no photoelectrons are produced, giving a minimum in the photoemission spectrum.

Ordinary surface plasmons of frequency  $\omega_p/\sqrt{2}$  cannot be produced by an incident photon in a perfect surface, as the lightline and surface plasmon dispersion relations have

no points in common on the  $\omega$  vs.  $q$  plane due to retardation effects ( $q$  is the momentum parallel to the surface).

Multipole modes associated with oscillating charge fluctuation in the direction perpendicular to the surface are the ideal candidates to be the main components in the non-zero contribution related to the divergence term.

It has been proved that, in contrast to the ordinary surface modes, multipole modes are very sensitive to the electronic structure at the surface<sup>1</sup>.

The ordinary surface modes reflect bulk properties and at  $q = 0$  their energy has only Coulomb contribution. However, even at  $q = 0$  multipole modes have kinetic contribution in addition to the Coulomb part, giving information about local properties.<sup>10</sup> Several approximations of the surface region have been published in an attempt to model the most important part of the response of the system. Some use the hydrodynamic model<sup>1,11-13</sup> and others use microscopic calculations<sup>14-16</sup> in which the photon field is screened with the same potential step as the one used to obtain the electronic wave functions.

Here we improve a previous two-step profile calculation<sup>9</sup> using a soft electronic profile to avoid the discontinuities at the vacuum-layer and layer-bulk boundaries that could be related with artificial enhancement of the photoemission spectrum.

A self-consistent screening of the field is performed using an analytical expression for the ground state density.

This paper is organized as follows. The photoemission formulation is presented in Sec. 2. Section 3 contains the calculation of the screened field and Sec. 4 contains the results and conclusions.

## **2. Photoemission Formulation.**

We consider a semi-infinite simple metal with its surface perpendicular to the  $z$ -axis and confined to the  $z < 0$  half-space. The jellium model is assumed for the positive ionic density defined as

$$N(z) = \tilde{n}_0 \Theta(-z) , \tag{4}$$

where  $\tilde{n}_0 = 3/4\pi r_s^3$  is the constant bulk density,  $\Theta$  is the step function and  $r_s$  is the electron radius.

Taking advantage of the translational symmetry on the  $xy$ -plane, the photoemission flux of electrons that reach the detector per unit of the solid angle and per incident photon can be written as

$$\frac{dI}{d\Omega} = \frac{p_f \cos(\theta)}{\omega} \left| i(q + 2p_{\parallel i}) \int dz \phi_f f \phi_i + \int dz \phi_f j \phi_i + 2 \int dz \phi_f g \phi_i' \right|^2, \quad (5)$$

where we have followed the scheme developed by Mahan in Ref. 17 (with the addition of the term  $\nabla \cdot \mathbf{A} \neq \mathbf{0}$ , not considered in Mahan's formulation). In Eq. (5)  $\phi_i$  is the  $z$ -dependent part of the initial electronic state at the Fermi energy,

$$\Phi_i(\mathbf{r}) = e^{i\mathbf{p}_{\parallel i} \cdot \rho} \phi_i(\mathbf{z}), \quad \mathbf{r} = (\rho, \mathbf{z}), \quad (6)$$

where  $\mathbf{p}_{\parallel f} = \mathbf{p}_{\parallel i} + \mathbf{q}$  is the balance between the final and initial electronic momenta parallel to the surface and the parallel momentum  $\mathbf{q}$  supplied by the incident photon.

$$\Phi_f(\mathbf{r}) = e^{-i\mathbf{p}_{\parallel f} \cdot \rho} \phi_f(\mathbf{z}) \quad (7)$$

comes from the Green function of a free electron that propagates from the metal to the vacuum through the surface potential at a constant energy  $E_f$ , given by

$$E_f = E_i + \omega, \quad (8)$$

where  $E_i$  is the Fermi energy.

The functions  $\Phi_i$  and  $\Phi_f$  are solutions to the Schrödinger equation for the unperturbed Hamiltonian  $H_0$ .

The functions  $f$  and  $g$  are the  $x$ - and  $z$ -components of the screened electric field given by

$$\mathbf{E} = \frac{i\omega}{\mathbf{c}} \mathbf{A}, \quad (9)$$

and  $j = g'$  is the  $z$ -derivative of the  $z$ -component. The field components inside the integrals ( $f$ ,  $g$  and  $j$ ) are normalized to unit amplitude for the  $x$ -component of the

incident photon in vacuum. We consider  $p$ -polarized light ( $s$ -polarized light would not produce a longitudinal component inside the metal) with an angle of incidence  $\theta$  with respect to the normal to the surface.

Two modifications to Eq.(2.9) in Ref. 17 have been applied to obtain our Eq.(5). Both of them mimic the experimental conditions used to compare our results. The first is that we do not perform the integration over initial states as we keep the initial state fixed and change  $\phi_f$  as we scan the frequency. The second is the normalization of the output to the incident flux (photons/sec), given by

$$\frac{E_0^2 \cos(\theta)}{\omega}, \quad (10)$$

where  $E_0$  is the amplitude of the incident photon far from the surface in vacuum.

We stress that the electron crosses the surface as a free particle and the full many-body effects are considered in the dressed field.

By far the most cumbersome part of the calculation is the screening of the photon field. We will focus on this part in the next section.

### 3. Screening of the Photon Field.

Our initial system of equations, within the hydrodynamic model, is given by

$$\nabla(\nabla \cdot \mathbf{E}) - \nabla^2 \mathbf{E} = -\frac{1}{c^2} \left[ \frac{\partial^2 \mathbf{E}}{\partial t^2} + 4\pi \frac{\partial \mathbf{j}}{\partial t} \right], \quad (11)$$

$$\nabla \cdot \mathbf{E} = 4\pi(n - N), \quad (12)$$

$$\frac{\partial \mathbf{j}}{\partial t} = n\mathbf{E} - \beta \nabla n - \gamma \mathbf{j}, \quad (13)$$

for the three unknowns  $\mathbf{E}$ ,  $\mathbf{j}$  and  $n$ ;  $n$  and  $\mathbf{j}$  are the electronic density and current respectively ( $\mathbf{j} = n\mathbf{v}$ ),  $N$  is the ionic density given by Eq. (4),  $\beta = \frac{3}{5}v_F^2$ ,  $v_F(z)$  being the local Fermi velocity and  $\gamma = \omega_p(z)/d$  is the damping parameter. The value  $d = 50$  has been used in the present work.

In order to linearize the equations we consider

$$n = n_0 + n_1 \exp(-i\omega t) \quad , \quad (14)$$

$$\mathbf{E} = \mathbf{E}_0 + \mathbf{E}_1 \exp(-i\omega t) \quad , \quad (15)$$

$$\mathbf{v} = \mathbf{v}_1 \exp(-i\omega t) \quad , \quad (16)$$

$$\beta = \beta_0 + \beta_1 \exp(-i\omega t) \quad , \quad (17)$$

$$\gamma = \gamma_0 + \gamma_1 \exp(-i\omega t) \quad , \quad (18)$$

which gives by substitution in the previous system,

$$\nabla(\nabla \cdot \mathbf{E}_0) - \nabla^2 \mathbf{E}_0 = 0 \quad , \quad (19)$$

$$\nabla \cdot \mathbf{E}_0 = 4\pi(n_0 - N) \quad , \quad (20)$$

$$n_0 \mathbf{E}_0 = \beta_0 \nabla \mathbf{n}_0 \quad (21)$$

to zeroth order in the perturbation, and

$$\nabla(\nabla \cdot \mathbf{E}_1) - \nabla^2 \mathbf{E}_1 = \frac{\omega^2}{c^2} \mathbf{E}_1 + \frac{4\pi i \omega}{c^2} \mathbf{n}_0 \mathbf{v}_1 \quad , \quad (22)$$

$$\nabla \cdot \mathbf{E}_1 = 4\pi n_1 \quad , \quad (23)$$

$$-i\omega n_0 \mathbf{v}_1 = n_0 \mathbf{E}_1 + \mathbf{n}_1 \mathbf{E}_0 - \beta_0 \nabla \mathbf{n}_1 - \beta_1 \nabla \mathbf{n}_0 - \gamma_0 \mathbf{n}_0 \mathbf{v}_1 \quad (24)$$

to first order in the perturbation.

The standard procedure would be to solve the zeroth order system obtaining the ground state density  $n_0$  from a given ionic distribution. Instead, we proceeded in a different way: we chose a well justified analytic electronic ground state profile and calculated  $\mathbf{E}_0$  from Eq. (21).

In the case of aluminum, the analytic form

$$n_0(z) = \frac{\tilde{n}_0}{e^{z/\delta} + 1} \quad , \quad (25)$$

with  $\delta = 0.66$  a.u. agrees well with the profile obtained from the Kohn Sham calculation presented in Ref. 18, see Fig. 1. This electronic profile together with

$$V(z) = - \int E_0 dz \quad , \quad (26)$$

where

$$\mathbf{E}_0 = \frac{3}{5}(\mathbf{3}\pi^2)^{2/3} \mathbf{n}'_0 \mathbf{n}_0^{-1/3} \mathbf{e}_z \quad , \quad (27)$$

obtained from Eq. (21), completely characterize the ground state of the system. In Eq. (27)  $\mathbf{e}_z$  is a unit vector along the  $z$ -axis and  $\mathbf{n}'_0 = dn_0/dz$ .

After some manipulations in the first-order system, we obtain the equations

$$a_1 f + a_2 f'' + a_3 g' = 0 \quad , \quad (28)$$

$$b_1 f + b_2 f' + b_3 g + b_4 g' + b_5 g'' = 0 \quad ; \quad (29)$$

the  $z$ -dependent coefficients  $a_i$  and  $b_i$  are given in the Appendix.

This coupled system of second order differential equations can be transformed into an equivalent fourth order equation for one variable or, alternatively, into a first-order system of equations for the four functions  $y_1(z), \dots, y_4(z)$ , defined as  $f = y_1$ ,  $f' = y_2$ ,  $g = y_3$  and  $g' = y_4$ , which satisfy

$$y'_1(z) = y_2(z)quad, \quad (30)$$

$$y'_2(z) = A_1 y_1(z) + A_3 y_4(z)quad, \quad (31)$$

$$y'_3(z) = y_4(z)quad, \quad (32)$$

$$y'_4(z) = B_1 y_1(z) + B_2 y_2(z) + B_3 y_3(z) + B_4 y_4(z)quad, \quad (33)$$

which must be solved numerically. The  $z$ -dependent coefficients  $A_i$  and  $B_i$  are defined as

$$A_i = -a_i/a_2 \quad B_i = -b_i/b_5 \quad (34)$$

and are given in the Appendix. The fields were integrated from inside using the “odeint” and “stiff” subroutines given in Ref. 19. These codes change the size of the integration step according to the nature of the profile and appeared to be the appropriate method for our stiff profile.

The main difficulty lies in the consideration of the boundary conditions. Deep inside the metal at  $z_1 < 0$ , where the electronic density becomes a constant function, the four independent analytical solutions are known: two longitudinal and two transverse plane wave functions moving in opposite directions.

Let us define the coefficients  $C_i$  within a general solution inside this region as

$$f(z) = C_1 e^{-ik_1 z} + C_2 e^{-ik_2 z} + C_3 e^{ik_1 z} + C_4 e^{ik_2 z} \quad , \quad (35)$$

where

$$k_1 = \left[ \frac{\omega^2}{c^2} \left( 1 - \frac{\omega_{p0}^2}{\omega(\omega + i\gamma_0)} \right) - q^2 \right]^{1/2} \quad , \quad (36)$$

$$k_2 = \left[ \frac{\omega(\omega + i\gamma_0) - \omega_{p0}^2}{\beta_0} - q^2 \right]^{1/2} \quad (37)$$

are  $z$ -components of the transverse and longitudinal wave vectors at  $z_1$ . The roots with  $\text{Im}(k_i) > 0$  have been used.

The absence of incoming waves from  $-\infty$  gives the first two of the boundary conditions, i.e.,  $C_3 = C_4 = 0$ .

Far from the surface in vacuum at  $z_2 > 0$ , where the density can be considered as a negligible constant function, the general analytical solution is given by

$$f(z) = D_1 e^{ikz} + D_2 e^{-ikz} + D_3 e^{ik_3 z} + D_4 e^{-ik_3 z} \quad (38)$$

where  $k$  and  $k_3$  are the  $z$ - components of the transverse and longitudinal wave vectors respectively. They are obtained from equations similar to Eqs. (36), and (37) using the values of  $\omega_p$ ,  $\gamma$  and  $\beta$  at  $z_2$ . We used the condition  $n(z_2)/\tilde{n}_0 = 10^{-8}$  and  $z_1 = -z_2$  to fix the  $z_i$  values. The remaining two boundary conditions must be the cancelation of both longitudinal solutions at  $z_2$ , or  $D_3 = D_4 = 0$ . In this way, the allowed radiation in vacuum is the incoming and reflected photon.

The application of boundary conditions at different points in space does not always have a solution, as the system must be compatible with them. In a numerical problem, this compatibility is a problem of relative accuracy. Taking advantage of the linear character of the system of equations, we inspected the  $4 \times 4$  matrix  $M$  that relates the analytical solutions at  $z_1$  and  $z_2$  and is given by

$$D = MC \quad . \quad (39)$$

The result of the inspection was that the matrix has a  $2 \times 2$  box of nearly zero elements, those denoted by  $m_{31}, m_{32}, m_{41}$  and  $m_{42}$ . This box produces negligible  $D_3$  and  $D_4$  coefficients for arbitrary values of  $C_1$  and  $C_2$ . However, we verified that the results were much more stable if we nonetheless imposed the two last boundary conditions using the “shooting method”.<sup>19</sup>

Figures 2 and 3 show the  $z$ -component of the vector potential as a function of  $z$ , normalized to the constant transverse component at  $z_1$ . In addition to the general discussion that we will include in the next section, some comments about the behavior of the fields due to screening effects in the region where the electronic density is negligibly small must be included here.

Rapid oscillations of the  $z$ -component of the vector potential appear in the region where the electronic density has nearly disappeared (see Fig.1 for comparison). The main reason for this unphysical behavior is attributable to the hydrodynamic model we are using, which fails to reproduce the correct response when the electronic density is negligible. For the longitudinal component (which represents the collective excitation of the system), the dispersion relation in a homogeneous system is given by

$$\omega(\omega + i\gamma) = \omega_p^2 + \beta(q^2 + k_3^2). \quad (40)$$

As the density goes to zero locally,  $\beta$ ,  $\gamma$  and  $\omega_p$  also tend to zero. However,  $\omega$  and  $q$  are finite quantities fixed by the incoming photon with which the system resonates. The only way to satisfy this equation is by a strong increase in  $k_3$ ; indeed, it must grow to infinity to compensate for the vanishing of the  $\beta$  coefficient. However, the consequences of these oscillations are not important, since the amplitude of the field tends to zero. This assertion is proved in the comparison shown in Fig. 4, as discussed in the next Section.

This annoying effect could be avoided by the introduction of an extra term in the dispersion relation, the well known  $K^4/4$  ( $\mathbf{K} = (\mathbf{q}, \mathbf{k}_3)$ ) term,<sup>20</sup> related with electron-hole excitations (and coming from the kinetic term within the Hamiltonian), which dominates the dispersion relation for high energy and large momentum transfer. If this term is

included, as the ground state density tends to zero,  $k_3$  converges to a finite value given by  $k_3^2 = 2\omega - q^2$  and the strong oscillations would disappear.

As was recently suggested in Ref. 21 this term can be obtained within the hydrodynamic model for a homogeneous electron gas from the material equation if the local equilibrium approximation is relaxed and extra terms coming from higher momenta of the distribution function are included. We tried with two different extra terms within the material equation built up from the polarization vector ( $\nabla \cdot \mathbf{P} = -\mathbf{n}$ ), one of them free of shear forces and given by  $\nabla(\nabla^2 \mathbf{n})$ , and the other one containing shear forces and given by  $(\nabla^2)^2 \mathbf{P}$ . These two terms include all the possible vector components that contain four derivatives of  $\mathbf{P}$ . They both imply the dispersion relation given by:

$$\omega(\omega + i\gamma) = \omega_p^2 + \beta(q^2 + k_3^2) + \frac{1}{4}(q^2 + k_3^2)^2 \quad (41)$$

which reproduces the random phase approximation result of Ref. 22. Both produce a new system of six coupled first-order equations which need six boundary conditions. The difficulty comes from the fact that two of the four solutions of  $k_3$  in Eq. (41) are unphysical, as for them  $\text{Im}(k_3) \cdot \text{Re}(k_3) < 0$ , which corresponds to a plane wave that diverges in the forward direction producing divergent solutions as the differential equation is solved from  $z_1$  to  $z_2$ . The goal of our future work is to find the appropriate term in the material equation that would leave the system linear and simultaneously produce well-behaved solutions of the dispersion relation.

#### 4. Results and Conclusions.

The physical parameters of our problem are the width of the surface profile given by  $\delta$ , the angle  $\theta$  between the incident photon and the normal to the surface, the angle  $\epsilon$  between the outgoing electron and the normal to the surface and the electron radius  $r_s$ .

In Figs.2 and 3 the  $z$ -component of the vector potential is shown as a function of  $z$  for different values of  $\omega$ . It has been normalized to the transverse component at  $z_1$  and consequently the deviation from 1 (of the real part) gives an idea of the importance of

the longitudinal component deep inside the metal. It can be observed that even though  $\text{Im}(k_2) \gg \text{Im}(k_1)$  and so strong damping is expected, its presence is significant at large distances from the surface and cannot be ignored for  $\omega > \omega_p$ .

Some characteristic features that were previously reported by Feibelman<sup>15</sup> within a self consistent calculation are reproduced here by us:  $\omega = \omega_p$  is the critical value from which the wave vector of the longitudinal component has a nonvanishing real part and consequently it penetrates the metal, producing decaying oscillations towards  $-\infty$ . For this value of  $\omega$  the amplitude of the nearly structureless field shows an abrupt decrease, producing a minimum (it should be zero if  $\gamma = 0$ , i.e. if no damping is considered) in the photoemission spectrum. For  $\omega < \omega_p$  there is a strong peak near  $z = 0$  produced by screening, a feature that strongly deviates from the classical optical calculation. Correlating the strength of the surface photoeffect with the intensity of the vector potential within the surface region, one would expect it to be large below  $\omega_p$  and much smaller above  $\omega_p$ .

Indistinguishable results were obtained when the selfconsistent density shown in Fig.1 was used.

In order to see the influence of the oscillations of the field at the vanishing density region on our results, we compare in Fig.4 for  $\delta = 0.2$  a.u. (which mimics an abrupt electronic profile) the evolution with  $\omega$  of the two transmission coefficients,  $C_1$  (transverse component) and  $C_2$  (longitudinal component) and the reflection coefficient  $D_1$  with those obtained analytically from a calculation that assumes a single step, structureless surface. The analytical coefficients are given in Ref. 23 by

$$C_{1c} = \frac{2k k_1}{t q} \quad , \quad (42)$$

$$C_{2c} = \frac{2k(\epsilon - 1) q}{t k_2} \quad , \quad (43)$$

$$D_{1c} = \frac{\epsilon k - k_1 + (\epsilon - 1)q^2/k_2}{qt} \sqrt{\frac{\omega^2}{c^2} - q^2} \quad , \quad (44)$$

where

$$t = \epsilon k + k_1 - (\epsilon - 1)q^2/k_2 \quad , \quad (45)$$

$$\epsilon = 1 - \frac{\omega_p^2}{\omega(\omega + i\gamma)} \quad , \quad (46)$$

and  $k$ ,  $k_1$ ,  $k_2$  are defined in Eqs. (36), (37) and (38). The curves do not show any structure, except at  $\omega_p$  and at  $\omega_p/\cos(\theta)$ , where the transverse component can penetrate the solid. The coincidence of the two results proves that the strong oscillations at the edge region shown in Figs. 2 and 3 do not affect the behavior of the field amplitudes as functions of  $\omega$ .

The same coincidence is obtained if  $r_s = 6$  is used, keeping all the other parameters fixed.

Figure 5 shows the change of the longitudinal transmission coefficient  $C_2$  [see Eq. (35)] as the electronic profile becomes less abrupt. As  $\delta$  increases, giving a flatter profile, a wide peak at about  $\omega = 0.75 \omega_p$  evolves. Apparently, the position of the peak is nearly insensitive to the changes in the electronic profile.

Finally, we centered on the study of the photoemission intensity per unit of the solid angle and incident photon for  $p$ -polarized light as a function of the photon frequency. The initial state  $\Phi_i$  is at  $E_i = -0.1615$  a.u. . This energy was chosen to reproduce the threshold value of  $\omega$  for aluminum. We take the zero of energy to be at vacuum level. No final state effects are taken into account. This last approximation is supported by experiment as no qualitative difference is observed between photoemission spectra made on different surfaces of aluminum crystals, suggesting that in a nearly free electron metal the screening effects are much greater than the structure produced by band effects.<sup>6</sup>

The finite mean free path of the emitted electron inside the metal has been modeled by a decreasing exponential factor multiplying the initial electronic wave function which ensures that only electrons coming from the last 50 Å will be considered.

Figure 6 shows the main result that must be compared with the experimental outputs,<sup>6</sup> (for  $\theta = \pi/4$ ,  $\epsilon = 0$  and  $\delta = 0.66$  a.u.). The main peak is centered at  $\omega = 0.77 \omega_p$ , in excellent agreement with the experimental peak position. The second peak, at  $\omega > \omega_p$ , has a shape comparable to the experimental one, though it has greater intensity. This too high intensity is caused by the absence of electron-hole excitation

processes from the hydrodynamic model. Thus, our model lacks the Landau damping mechanism, through which the collective excitations can decay into electron-hole pairs. This type of damping would have a significant effect only for  $\omega > \omega_p$ , where the bulk plasmons created by the incident photon can overlap the electron-hole band and disappear, thus causing the photoemission efficiency in this region to decrease. Unlike the surface modes at  $\omega < \omega_p$ , these bulk plasmons can have a high enough perpendicular momentum, to enable this process.

More recent experimental data reported in Ref. 7 show the main peak at  $\omega = 0.85 \omega_p$ .

To gain insight into the physical significance of the main peak, we fixed  $\delta = 1.2$  a.u.,  $\epsilon = 0$  and  $r_s = 2.07$  and looked for the variation of the spectra for different values of the direction of the incident photon (given by  $\theta$ ). A large value of  $\delta$  was chosen to increase the probability of multipole modes. As shown in Fig. 7, the peak position turns out to be sensitive to the value of  $\theta$ . The peak disperses to lower energies as  $q_{\parallel}$  increases.

A peak produced by a multipole mode should hardly disperse (for these small values of  $q$ ) and, in any case, according to previous calculations,<sup>3</sup> it would disperse in the opposite direction. Our results indicate that the main peak need not be a direct manifestation of multipole modes, as has been asserted in the literature,<sup>8</sup> using the coincidence in energy as the main argument.

Another known difficulty concerning the identification of the main photoemission peak with the multipole modes, is that the RPA calculation of the photoemission spectrum<sup>15</sup> predicts that the frequency of this peak should increase with  $r_s$ . However, the results of measurements of the multipole modes frequency by electron loss spectroscopy do not follow this trend.

In order to understand the origin of the  $\theta$  dependence of  $dI/d\Omega$ , let us analyze the different contributions to Eq. (5). On the right hand side, the first two terms come from  $\nabla \cdot \mathbf{A}$  and the third comes from  $\mathbf{A} \cdot \nabla$ . If  $\mathbf{A}$  is a constant field, only the third term will be nonzero and the  $\theta$ -dependent term will be a global factor that will change the intensity of  $dI/d\Omega$  for different  $\theta$  values, but not its shape. If  $\mathbf{A}$  is not a constant field,

the three terms will survive and as their relative weights are  $\theta$  dependent, changes on  $\theta$  also produce changes in the shape of the  $(dI/d\Omega)/\omega$  function.

Moreover, though the contribution of the first two terms is significant, the greatest contribution comes from the third term, as shown in Fig. 6 (dashed line), where the first two terms of Eq. (5) have been removed.

We now compare our results with those of two sets of experimental data, in which the angular dependence of the photoemission was displayed. In the case of indium,<sup>24</sup> our calculated results for the main peak agree reasonably well with the measured ones. The measured peak moves from about  $0.84 \omega_p$  to about  $0.92 \omega_p$ , as  $\theta$  changes from  $45^\circ$  to  $15^\circ$ , whereas the corresponding calculated peak position moves from  $0.77 \omega_p$  to  $0.92 \omega_p$  for the same angle variation. These measurements were not extended to  $\omega > \omega_p$ , so we cannot perform any comparisons in this region. For Al, on the other hand, the recent experimental data of Barman *et al.*<sup>7</sup> cover the frequency regions both above and below  $\omega_p$ . Experimentally, the main peak, below  $\omega_p$ , exhibits no dispersion when  $\theta$  changes, unlike the calculated results. For  $\omega > \omega_p$  there appear in the measured data two minor peaks (called features A and B in Ref. 7), which also occur in our calculated results. The arrows in Figs. 6 and 7 denote the positions of the high energy peaks, which disperse in the same way as the experimental data (feature A of Ref. 7). The vertical line at about  $\omega/\omega_p = 1.07$  denotes the position of the minor peak (for  $\theta = 50^\circ$  and  $\theta = 70^\circ$ ) which does not disperse (feature B in Ref. 7).

In conclusion, we have presented an analytical calculation of the photoemission spectrum and its dependence on the photon angle of incidence. The screening of the photon field, including nonlocal effects and excitation of longitudinal modes, was calculated within a hydrodynamic model with a realistic surface density profile. Our results indicate that the main peak, below  $\omega_p$ , need not be just due to multipole mode excitation. The two sets of experimental data with which we compared our results seem to be contradictory as regards the main peak dispersion. Thus, further experiments on other materials are needed to resolve this question.

## Appendix A

Here we give the definitions of the coefficients  $a_i$  and  $b_i$ :

$$a_1(z) = \omega^2(\omega + i\gamma_0(z)) - \omega[4\pi n_0(z) + q^2\beta_0(z)]quad, \quad (47)$$

$$a_2(z) = c^2(\omega + i\gamma_0(z))quad, \quad (48)$$

$$a_3(z) = iq[\omega\beta_0(z) - c^2(\omega + i\gamma_0(z))]quad, \quad (49)$$

$$b_1(z) = i\omega q \left[ \frac{2}{3}\beta_0(z)\frac{n'_0(z)}{n_0(z)} - E_0(z) \right] quad, \quad (50)$$

$$b_2(z) = a_3(z)quad, \quad (51)$$

$$b_3(z) = -4\pi n_0(z)\omega - (\omega + i\gamma_0(z))(c^2q^2 - \omega^2)quad, \quad (52)$$

$$b_4(z) = \omega \left[ \frac{2}{3}\beta_0(z)\frac{n'_0(z)}{n_0(z)} - E_0(z) \right] quad, \quad (53)$$

$$b_5(z) = \beta_0(z)\omega \quad , \quad (54)$$

$$\gamma_0 = \frac{(4\pi n_0)^{1/2}}{50} \quad , \quad (55)$$

$$\beta_0 = \frac{3}{5}(3\pi^2 n_0)^{2/3} \quad . \quad (56)$$

The coefficients  $A_i$  and  $B_i$  defined in Eq. (34) are given by

$$A_1(z) = -\frac{\omega^2}{c^2} \left[ 1 - \frac{4\pi n_0(z) + q^2\beta_0(z)}{\omega(\omega + i\gamma_0(z))} \right] \quad , \quad (57)$$

$$A_3(z) = -iq \left[ \frac{\omega\beta_0(z)}{c^2(\omega + i\gamma_0(z))} - 1 \right] \quad , \quad (58)$$

$$B_1(z) = -iq \frac{1}{3\delta\tilde{n}_0} n_0(z) e^{z/\delta} \quad , \quad (59)$$

$$B_2(z) = -iq \left[ 1 - \frac{c^2}{\omega} \frac{\omega + i\gamma_0(z)}{\beta_0(z)} \right] \quad , \quad (60)$$

$$B_3(z) = \frac{20\pi}{3(3\pi^2)^{2/3}} n_0(z)^{1/3} + \frac{\omega(\omega + i\gamma_0(z))}{\beta_0(z)} \left( \frac{c^2q^2}{\omega^2} - 1 \right) \quad , \quad (61)$$

$$B_4(z) = -\frac{1}{3\delta\tilde{n}_0} n_0(z) e^{z/\delta} \quad . \quad (62)$$

## Acknowledgments

This work was supported in part by the Comisión Asesora de Investigación Científica y Técnica (CAICYT), Spain under Grant No. PB95-1249, DGICYT PB 94-0215 and

CIRIT 1998SGR-00042. One of the authors (S.N.) wishes to express his gratitude for the warm hospitality during his stay at the Department ECM, Fisica, Universitat de Barcelona.

## FIGURE CAPTIONS

Fig. 1 Ground state density for aluminum. The solid line is the self consistent calculation taken from Ref.<sup>18</sup> and the dashed line is the analytical function given in Eq. (25) for  $\delta = 0.66 \text{ a.u.}$ . All figures are calculated for  $r_s = 2.07 \text{ a.u.}$ .

Fig. 2 (a) Real and (b) imaginary parts of the  $z$ -component of the vector potential  $vs. z$  calculated for different values of  $\omega \leq \omega_p$ . The normalization constant  $A_z^T$  is the transverse component at  $z_1$ .  $\delta = 0.66 \text{ a.u.}$ , and  $\theta = \pi/4$  were used.

Fig. 3 Same as Fig. 2 for  $\omega \geq \omega_p$ .

Fig. 4 Variation of the real and imaginary parts of the coefficients  $C_1$ ,  $C_2$  and  $D_1$  (see Eqs. (35) and (38)) with  $\omega$  for  $\delta = 0.2 \text{ a.u.}$ , and  $\theta = \pi/4$ . Insets: the same coefficients for a structureless surface.

Fig. 5 Variation of the real part of the longitudinal coefficient  $C_2$  with  $\omega/\omega_p$  for different values of  $\delta$ .  $\theta = \pi/4$  was used.

Fig. 6 Photoemission spectrum as a function of  $\omega/\omega_p$  for  $\delta = 0.66 \text{ a.u.}$ ,  $\epsilon = 0$  and  $\theta = \pi/4$ . A partial contribution to the spectrum is included as a dashed curve (see text). The arrow is at  $\omega_p/\cos(\theta)$ .

Fig. 7 Variation of the photoemission spectrum with  $\theta$  for  $\delta = 1.2 \text{ a.u.}$  and  $\epsilon = 0$ . The arrows are at  $\omega_p/\cos(\theta)$ .

## REFERENCES

- <sup>1</sup> A.J. Bennett, Phys. Rev. **B1**, 203 (1970).
- <sup>2</sup> K.D. Tsuei, E.W. Plummer, A. Liebsch, K. Kempa and P. Bakshi, Phys. Rev. Lett. **64**, 44 (1990).
- <sup>3</sup> K.D. Tsuei, E.W. Plummer, A. Liebsch, E.Pehlke, K. Kempa, P. Bakshi, Surf. Sci. **247**, 302 (1991).
- <sup>4</sup> F. Moresco, M. Rocca, V. Zielasek, T. Hildebrandt and M. Henzler, Phys. Rev. **B54**, 14333 (1996).
- <sup>5</sup> V.U. Nazarov, Phys. Rev. **B59**, 9866 (1999).
- <sup>6</sup> H.J. Levinson, E.W. Plummer, P.J. Feibelman, Phys. Rev. Lett. **43**, 952 (1979).
- <sup>7</sup> S.R. Barman, P. Häberle, K. Horn, Phys. Rev. **B58**, R4285 (1998).
- <sup>8</sup> E.W. Plummer, Solid State Comm. **84**, 143 (1992).
- <sup>9</sup> N. Barberan, J.Bausells, E. Ardiles, Surf. Rev. Lett. **5**, 527 (1998).
- <sup>10</sup> J. Sellares, N. Barberan, Phys. Rev. **B50**, 1879 (1994).
- <sup>11</sup> K. Kempa, F. Forstmann, Surf. Sci. **129**, 516 (1985).
- <sup>12</sup> A. Eguiluz, S.C. Ying, J.J. Quinn, Phys. Rev. **B11**, 2118 (1975).
- <sup>13</sup> C. Schwartz, W.L. Schaich, Phys. Rev. **B30**, 1059 (1984).
- <sup>14</sup> P.J. Feibelman, Phys. Rev. **B12**, 1319 (1975).
- <sup>15</sup> P.J. Feibelman, Phys. Rev. Lett. **34**, 1092 (1975).
- <sup>16</sup> D. Samuelson, W.Schattke, Surf. Sci. **327**, 379 (1995).
- <sup>17</sup> G.D. Mahan, Phys. Rev. **B2**, 4334 (1970).
- <sup>18</sup> E. Krotscheck, W. Kohn, Guo-Xin Qian, Phys. Rev. **B32**, 5693 (1985).

- <sup>19</sup> W.H. Press, B.P. Flannery, S.A. Teukolsky, W.T. Vetterling, 1994 Numerical Recipes (Cambridge University Press).
- <sup>20</sup> D. Bohm, D. Pines, Phys. Rev. **92**, 609 (1953).
- <sup>21</sup> I. Tokatly, O. Pankratov, cond-mat 9902316.
- <sup>22</sup> L. Hedin, S. Lundqvist, in Solid State Physics **23**, 1 (1969).
- <sup>23</sup> A.R. Melnyk, M.J. Harrison, Phys. Rev. **B2**, 835 (1970).
- <sup>24</sup> G. Jezequel, Phys. Rev. Lett. **45**, 1963 (1980).

## FIGURES

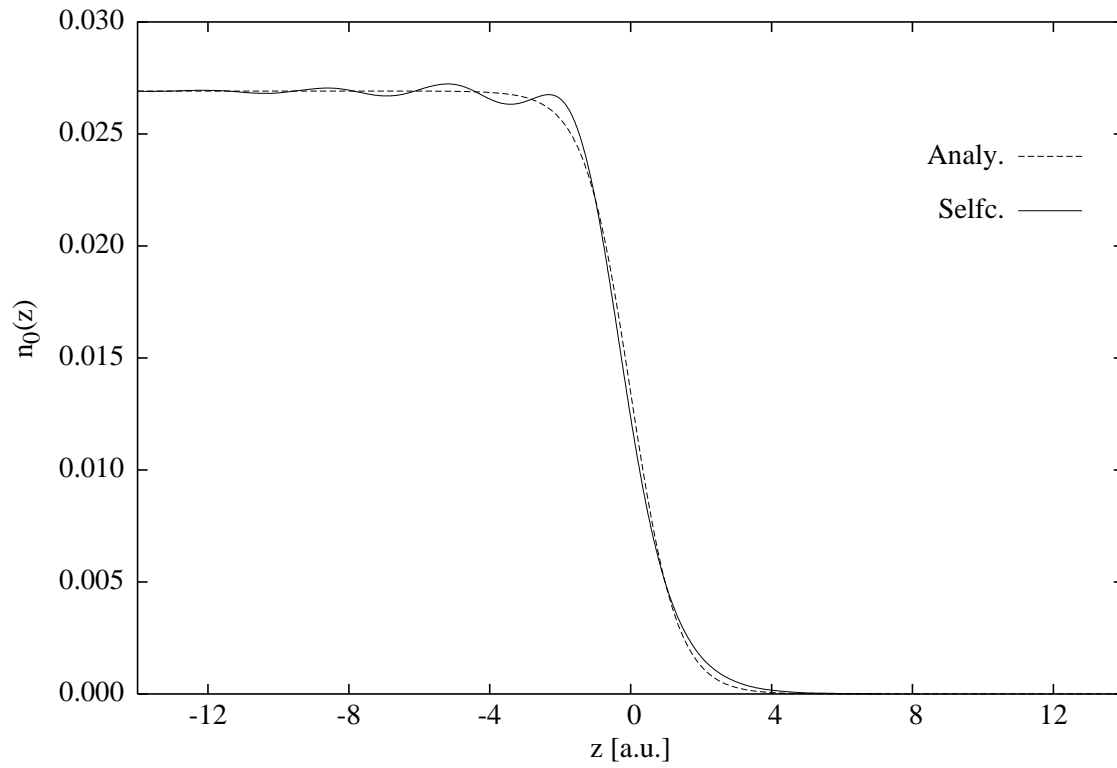


FIG. 1. Ground state density for aluminum. The solid line is the self consistent calculation taken from Ref. 18 and the dashed line is the analytical function given in Eq. (25) for  $\delta = 0.66$  a.u.. All figures are calculated for  $r_s = 2.07$  a.u..

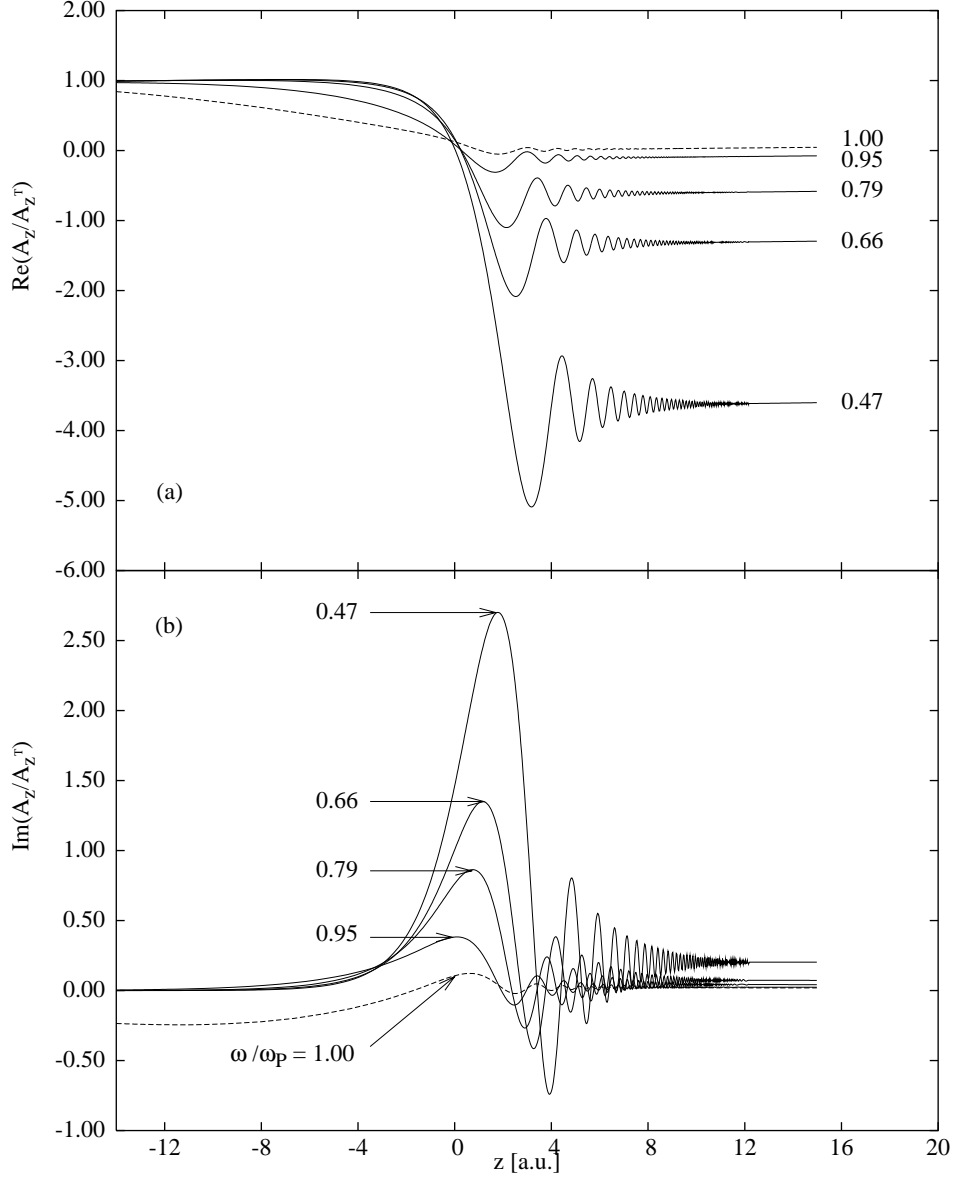


FIG. 2. (a) Real and (b) imaginary parts of the  $z$ -component of the vector potential  $vs.$   $z$  calculated for different values of  $\omega \leq \omega_p$ . The normalization constant  $A_z^T$  is the transverse component at  $z_1$ .  $\delta = 0.66$  a.u., and  $\theta = \pi/4$  were used.

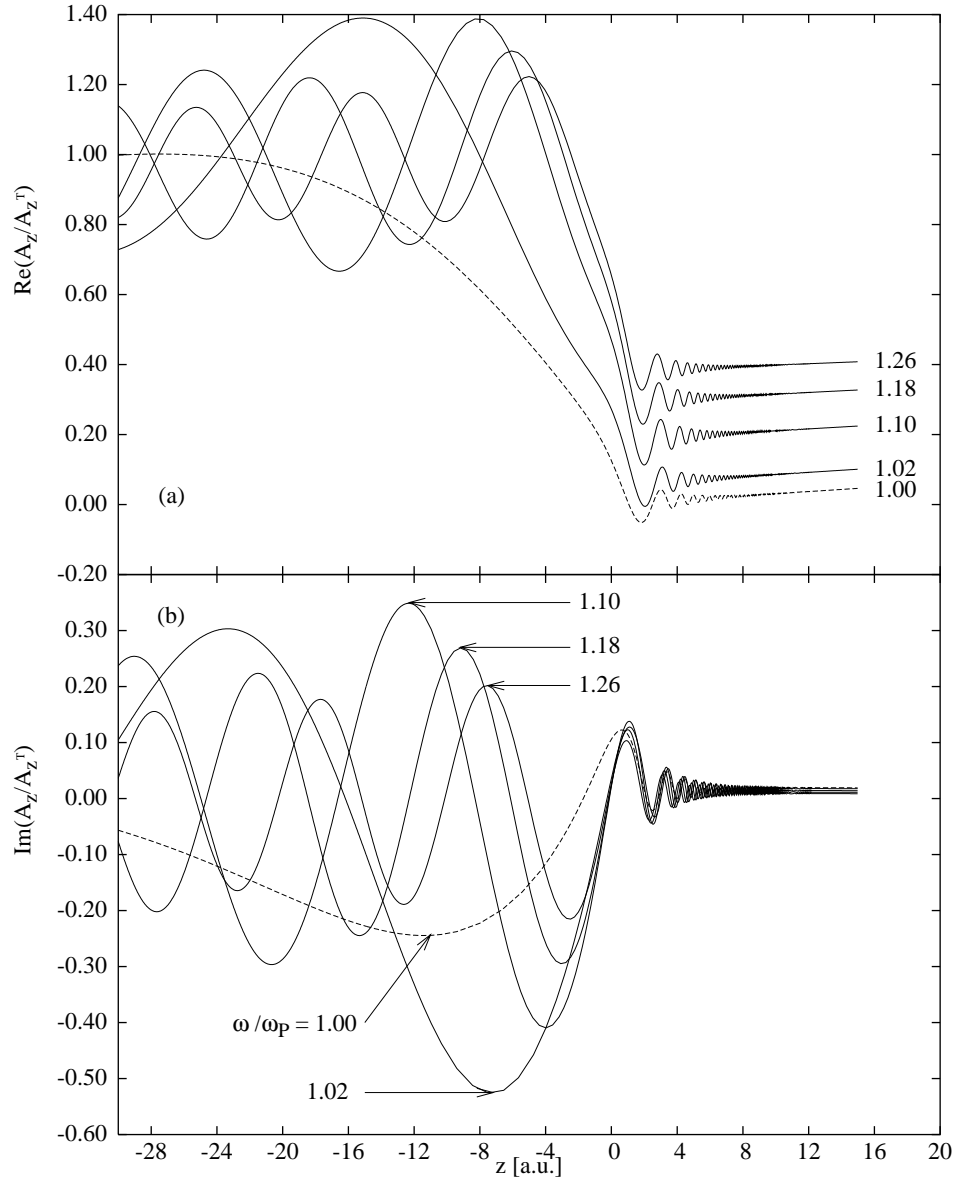


FIG. 3. Same as Fig. 2 for  $\omega \geq \omega_p$ .

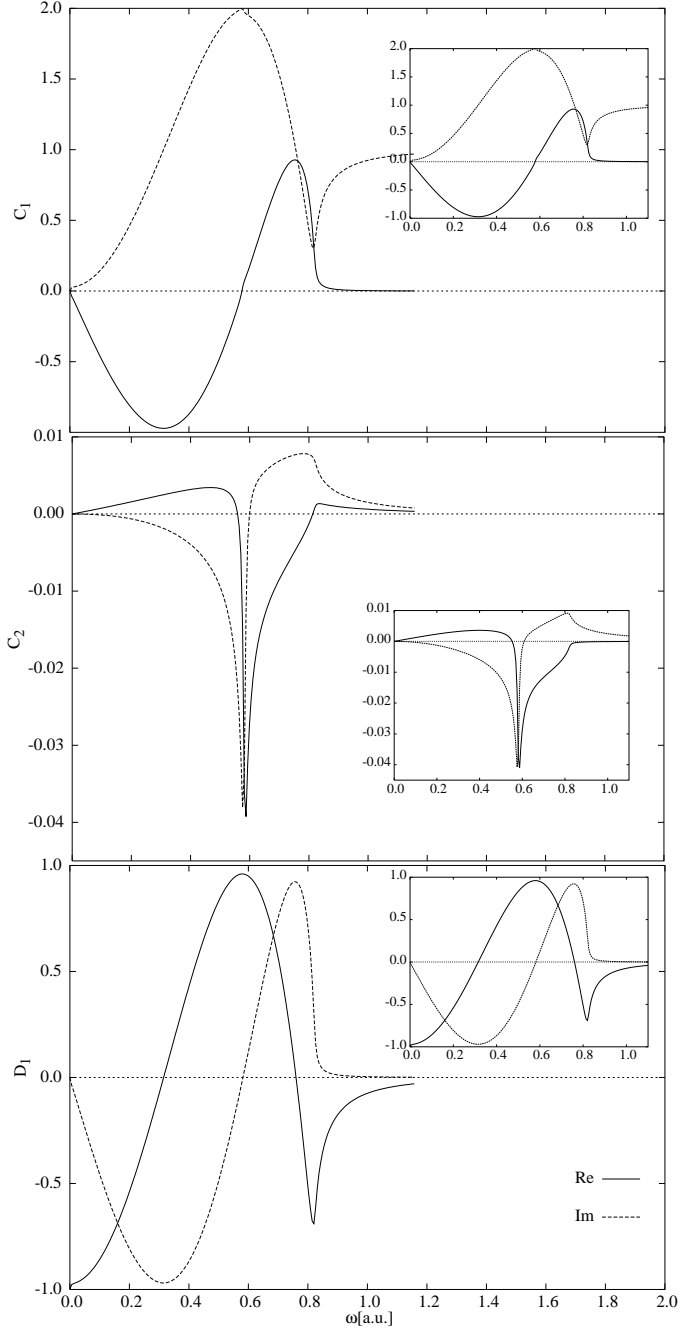


FIG. 4. Variation of the real and imaginary parts of the coefficients  $C_1$ ,  $C_2$  and  $D_1$  (see Eqs. (35) and (38)) with  $\omega$  for  $\delta = 0.2 \text{ a.u.}$ , and  $\theta = \pi/4$ . Insets: the same coefficients for a structureless surface.

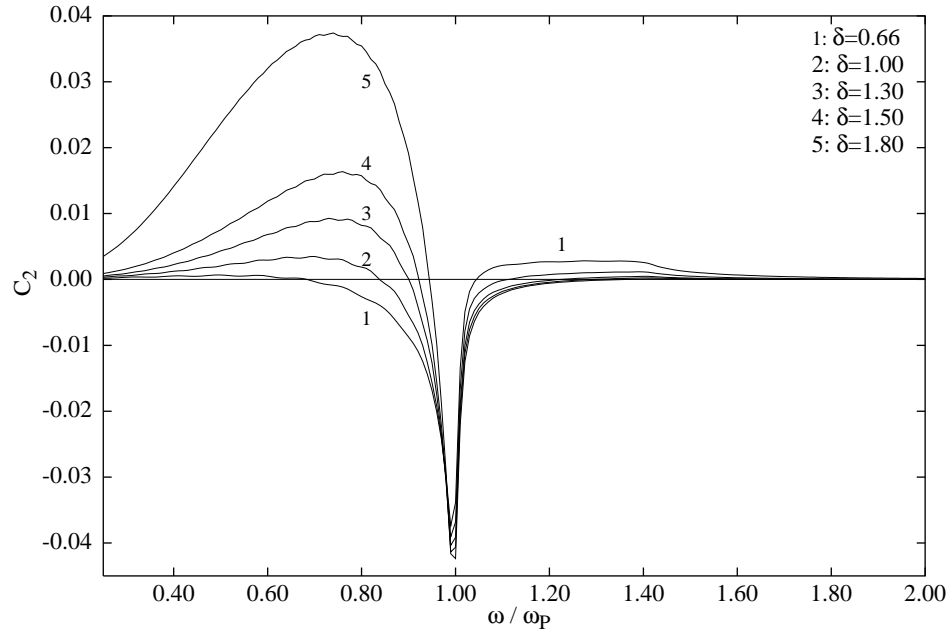


FIG. 5. Variation of the real part of the longitudinal coefficient  $C_2$  with  $\omega/\omega_p$  for different values of  $\delta$ .  $\theta = \pi/4$  was used.

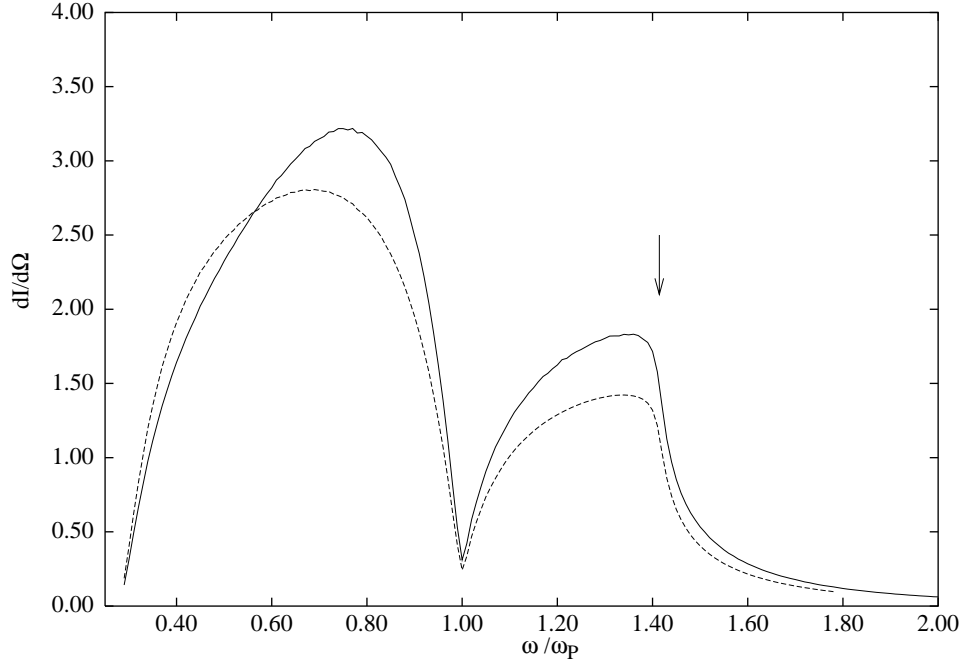


FIG. 6. Photoemission spectrum as a function of  $\omega/\omega_p$  for  $\delta = 0.66$  *a.u.*,  $\epsilon = 0$  and  $\theta = \pi/4$ . A partial contribution to the spectrum is included as a dashed curve (see text). The arrow is at  $\omega_p/\cos(\theta)$ .

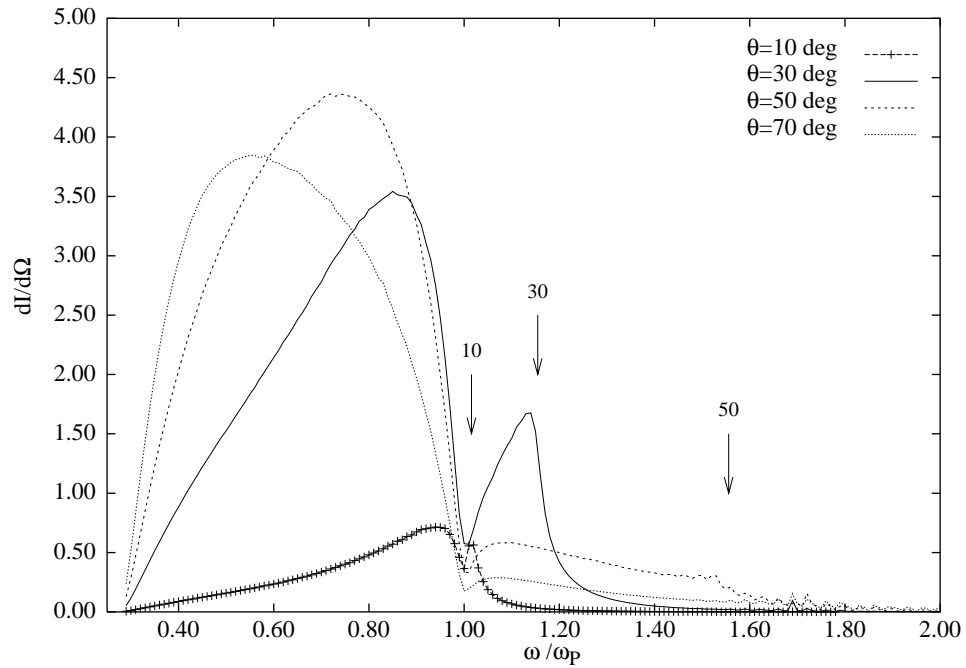


FIG. 7. Variation of the photoemission spectrum with  $\theta$  for  $\delta = 1.2$  *a.u.* and  $\epsilon = 0$ . The arrows are at  $\omega_p/\cos(\theta)$ .